

UC San Diego

UC San Diego Previously Published Works

Title

The Correlation between the Elastic Modulus of the Achilles Tendon Enthesis and Bone Microstructure in the Calcaneal Crescent

Permalink

<https://escholarship.org/uc/item/2wz9w4cm>

Journal

Tomography, 10(10)

ISSN

2379-1381

Authors

Doi, Kenichiro
Moazamian, Dina
Namiranian, Behnam
[et al.](#)

Publication Date

2024

DOI

10.3390/tomography10100122

Peer reviewed

Article

The Correlation between the Elastic Modulus of the Achilles Tendon Enthesis and Bone Microstructure in the Calcaneal Crescent

Kenichiro Doi ^{1,2,*} , Dina Moazamian ¹, Behnam Namiranian ¹, Sheronda Statum ^{1,3}, Amir Masoud Afsahi ¹ , Takuaki Yamamoto ² , Karen Y. Cheng ¹, Christine B. Chung ^{1,3} and Saeed Jerban ^{1,3,*} 

¹ Department of Radiology, University of California—San Diego, 9500 Gilman Drive, La Jolla, CA 92093, USA; kcheng@health.ucsd.edu (K.Y.C.); cbchung@health.ucsd.edu (C.B.C.)

² Department of Orthopedic Surgery, Faculty of Medicine, Fukuoka University, Fukuoka 810-0180, Japan

³ Radiology Service, Veterans Affairs San Diego Healthcare System—San Diego, La Jolla, CA 92161, USA

* Correspondence: k.doi.gm@adm.fukuoka-u.ac.jp (K.D.); sjerban@health.ucsd.edu (S.J.); Tel.: +1-858-246-2229 (S.J.)

Abstract: Background: The calcaneal entheses, an osseous footprint where the Achilles tendon seamlessly integrates with the bone, represents a complex interface crucial for effective force transmission. Bone adapts to mechanical stress and remodels based on the applied internal and external forces. This study explores the relationship between the elasticity of the Achilles tendon entheses and the bone microstructure in the calcaneal crescent. Methods: In total, 19 calcaneal-entheses sections, harvested from 10 fresh-frozen human cadaveric foot-ankle specimens (73.8 ± 6.0 years old, seven female), were used in this study. Indentation tests were performed at the entheses region, and Hayes' elastic modulus was calculated for each specimen. Micro-CT scanning was performed at 50-micron voxel size to assess trabecular bone microstructure within six regions of interest (ROIs) and the cortical bone thickness along the calcaneal crescent. Results: Significant Spearman correlations were observed between the entheses elastic modulus and trabecular bone thickness in the distal entheses (ROI 3) and proximal plantar (ROI 4) regions ($R = 0.786$ and 0.518 , respectively). Conclusion: This study highlights the potential impacts of Achilles tendon entheses on calcaneal bone microstructure, which was pronounced in the distal calcaneal entheses, suggesting regional differences in load transfer mechanism that require further investigation.

Keywords: achilles tendon; entheses; elastic modulus; calcaneal crescent; bone microstructure; micro-computed tomography



Citation: Doi, K.; Moazamian, D.; Namiranian, B.; Statum, S.; Afsahi, A.M.; Yamamoto, T.; Cheng, K.Y.; Chung, C.B.; Jerban, S. The Correlation between the Elastic Modulus of the Achilles Tendon Enthesis and Bone Microstructure in the Calcaneal Crescent. *Tomography* **2024**, *10*, 1665–1675. <https://doi.org/10.3390/tomography10100122>

Academic Editor: Emilio Quaia

Received: 14 August 2024

Revised: 7 October 2024

Accepted: 8 October 2024

Published: 10 October 2024



Copyright: © 2024 by the authors. Licensee MDPI, Basel, Switzerland. This article is an open access article distributed under the terms and conditions of the Creative Commons Attribution (CC BY) license (<https://creativecommons.org/licenses/by/4.0/>).

1. Introduction

The calcaneal entheses, an osseous footprint where the Achilles tendon seamlessly integrates with the bone, represents a complex interface crucial for effective force transmission between the muscular and skeletal systems [1]. The attachment between the tendon and bone occurs across a complex transitional tissue, called the entheses, that helps to reduce stress concentration at the tendon attachment site and facilitates efficient load transfer [2]. Compositional and architectural features of the entheses allow it to be uniquely adapted to the function of load transmission, with loads at some anatomical sites higher than body weight, over the course of millions of loading cycles [3–8]. According to previous studies, the trabecular bone structure at the entheses site is arranged in a specific direction, which enhances the efficiency of load transfer [9]. Furthermore, the tissue structure of the entheses, especially at the Achilles tendon attachment, is microstructurally adapted to maintain durability even under high-load conditions [10]. Degenerative changes in the tendon may alter the load distribution and transmission at the entheses, leading to structural adaptations or damage in the trabecular bone. These adaptations are particularly

notable in the Achilles tendon, which is responsible for bearing loads that often surpass body weight [11]. For example, in patients with Achilles tendinitis, fine damage to the enthesis and surrounding bone structure has been reported, which may cause further tendon degeneration and pain [12,13]. Therefore, understanding the relationship between the Achilles tendon enthesis and the trabecular bone is crucial for predicting biomechanical and pathophysiological mechanisms of the Achilles tendon and osseous structural remodeling. The main objective of this study is to investigate whether the mechanical properties of the Achilles tendon enthesis are associated with specific bone microstructural features in the calcaneal crescent and to determine if there are regional differences in such correlations.

Bone has the unique ability to adapt its structure and material properties according to the local mechanical environment [14]. Many *in vivo* mechanobiological experiments have shown that mechanical forces at the tissue level are able to drive local bone formation and resorption [15–19], leading to reconfigurations of cortical and trabecular bone morphology. Prior research has shown that mechanical loading stimulates bone remodeling, leading to alterations in both bone density and architecture [20–22]. The calcaneal crescent is an example of the trabecular bone's structural adaptation to the tensile and compressive forces it experiences, which aligns with the concept of Wolff's law [21,23,24]. According to Wolff's law, mechanical loading influences bone morphology and orientation, enabling it to effectively bear and transmit forces based on the direction and magnitude of these loads [22]. The bone beneath the calcaneal enthesis has the critical biomechanical task of receiving loads from the Achilles tendon and redistributing them away from the attachment point. In a histological study, Milz et al. reported that the calcaneal Achilles tendon attachment site showed a bone beam structure arranged in a fixed direction [9]. This arrangement of the bone beams is thought to enable efficient transmission and dispersion of loads. Previous studies have suggested that there is a close interplay between plantar fasciitis and the microstructural integrity of the calcaneal trabecular bone [23]. For example, Finkenstaedt et al. observed abnormalities in the trabecular structure of the calcaneus in patients with plantar fasciitis, suggesting that this may increase forces exerted onto the Achilles tendon–calcaneal crescent–plantar fascia system [24]. Varying mechanical properties of the Achilles tendon may arise due to specific structural and compositional adaptations in response to different functional demands. For instance, regional differences in fiber orientation, collagen content, and mineralization may contribute to such variations, reflecting the tendon's complex role in force transmission and load bearing during various activities [9,21,23,25]. However, it is still unclear how the mechanical properties of the Achilles tendon enthesis may correlate with the bone microstructure of the calcaneal crescent.

We hypothesized that the mechanical properties of Achilles tendon enthesis would affect the bone microstructure of the calcaneal crescent. The purpose of this *ex vivo* study is to investigate the correlations between the mechanical properties of Achilles tendon enthesis and the bone microstructure of the calcaneal endosteum. This study also explores the regional differences in such correlations within the calcaneal crescent. Additionally, we aim to verify the feasibility of measurement methods to examine the relationship between the elasticity of the Achilles tendon and the bone microstructure beneath the calcaneal enthesis. This study fills a gap in the existing research by revealing how regional variations in the mechanical properties of the Achilles tendon enthesis correlate with the bone microstructure of the calcaneal crescent. These findings contribute to a deeper understanding of the adaptive response of bone to varying mechanical forces at the tendon–bone interface.

2. Materials and Methods

2.1. Sample Preparation

This study was conducted in accordance with the Declaration of Helsinki and was approved by the Institutional Review Board of the University of California, San Diego (protocol code IRB: #804315).

Eleven fresh-frozen human cadaveric foot-ankle samples were obtained through the Medical Education and Anatomical Services of our institution. All cadaveric specimens were freshly frozen within 24 h post-mortem and stored at $-70\text{ }^{\circ}\text{C}$ until testing. Each specimen was subjected to only a single freeze-thaw cycle prior to experimentation to minimize potential adverse effects on tissue architecture. The storage time for these specimens was 3–6 months. All specimens were visually inspected for structural integrity before use. The distal and posterior portions of these specimens were sectioned into 4- to 6-mm thick sagittal slices, using a commercial bandsaw (B16, Butcher Boy Machines, Selmer, TN, USA) and a low-speed diamond saw (Isomet 1000, Buehler, IL, USA), ensuring the inclusion of the calcaneus bone, entheses, and a segment of the Achilles tendon. To rehydrate the specimens after any potential dehydration during the preparation process, the tendon-entheses sections were immersed in phosphate-buffered saline (PBS) for 2 h [26]. Skin, muscle, and adipose tissue were gently removed with a scalpel before mechanical testing.

The total number of sections was 28 (2–3 sections per donor). All specimens were visually examined, and all were found to be grossly normal. We excluded seven specimens with damaged trabecular bone observed in the micro-CT images performed later. The large bone defects were mostly due to the holders and screws used in the sectioning process with the Isomet saw. We also excluded two specimens in which the indentation-based elastic modulus could not be measured due to displacement of the indenter into the bone region. After these exclusions, 19 calcaneal-entheses sections from 10 fresh-frozen human cadaveric foot-ankle specimens (73.8 ± 6.0 years old at the time of death, seven female) were included in the analysis in this study (Figure 1).

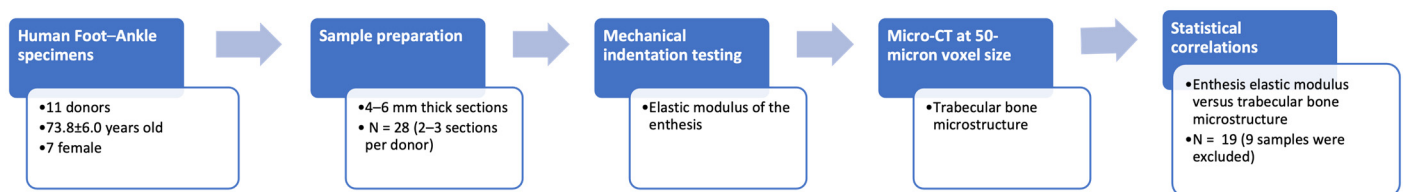


Figure 1. Flowchart illustrating the overall study design, including sample preparation, mechanical indentation testing, micro-CT imaging, bone microstructure analysis, and statistical correlation evaluation.

2.2. Mechanical Indentation Testing

Indentation testing was performed using a commercially available biomechanical testing system (MACH-1, Biomentum, Laval, QC, Canada). Specimens were placed in 5.08 cm square Petri dishes filled with PBS to avoid dehydration during mechanical testing. A flat-end cylindrical indenter with a 1.0 mm diameter was placed perpendicular to the specimen's cut surface. The entheses region of the specimens was tested at seven to ten points, each 2 mm apart, with the total number of testing points determined by the entheses length. Points were roughly 1–2 mm away from the bone surface to avoid bone influence on the results. Figure 2a shows the indentation test construct for measuring the mechanical properties of a representative Achilles tendon-entheses specimen (the entheses region is indicated with the dashed line red polygon).

For each test point, after finding the contact between the indenter tip and the tissue, the actuator was moved lower at a rate of $100\text{ }\mu\text{m/s}$. The maximum indentation depth was set to $300\text{ }\mu\text{m}$ (less than 10% of the minimum specimen thickness) to avoid significant nonlinearities in the tissue deformation. The average mechanical properties at each point were measured from two consecutive indentations with a 5-s pause in between. Figure 2b shows the load-displacement curve of a typical indentation test to determine the maximum load (P_{max}) required to calculate the Hayes' modulus (E) using Equation (1) [27].

$$E_{Hayes} = \frac{(1 - \nu^2)}{2ak} \frac{P_{max}}{depth} \quad (1)$$

where ν , a , P_{max} , $depth$, and k are Poisson's ratio, indenter radius, maximum load, indentation depth, and the correction factor ($k = 1.25$), respectively. The selection of the correction factor was based on the chart provided in the study of Hayes et al. [25], using the indenter diameter, indentation depth, and Poisson's ratio as guides. A Poisson's ratio of 0.45 was used in the calculations.

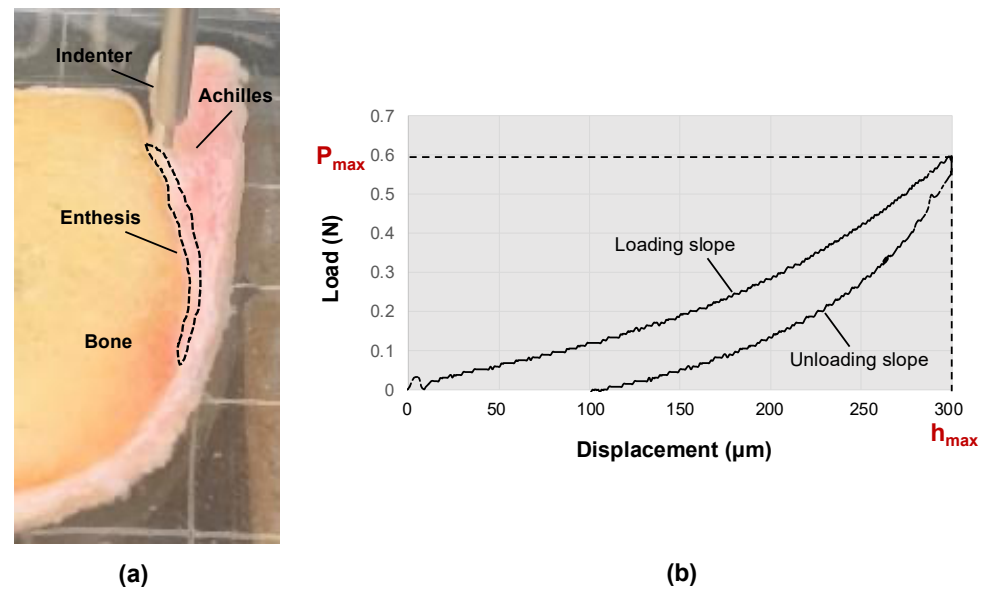


Figure 2. (a) Experimental setup for indentation test on a representative Achilles tendon-enthesis specimen using a commercial biomechanical testing system (MACH-1, Biomentum, QC, Canada). A flat-end cylindrical indenter with a 1.0 mm diameter was placed perpendicular to the specimen's cut surface. (b) Load-displacement curve of a typical indentation test to determine the maximum load (P_{max}) required to calculate the Hayes' elastic modulus (E).

2.3. Micro-Computed Tomography (Micro-CT) and Trabecular Microstructure

Bone specimens were scanned using a GE eXplore 120 Preclinical μ CT scanner (Waukesha, WI, USA) at 50 μ m isotropic voxel size. Other scanning parameters were as follows: 100 mm field of view, 60 kV voltage, 32 mA current, and 0.5° rotation step.

Bone microstructure was quantified from the micro-CT images using custom MATLAB scripts (version 2022, Mathworks, Natick, MA, USA). Bone Volume to Total Volume (BV/TV) was calculated as the ratio of trabecular bone volume to the total ROI volume. Trabecular bone thickness (Tb.Th) was measured as the average diameter of trabeculae in 3D space, while trabecular separation (Tb.Sp) was determined as the average diameter of spaces between trabeculae. Bone radiodensity in Hounsfield Units (HU) was assessed by converting the grayscale values from micro-CT images to HU using the scaling slope and intercept recorded in the image headers. Bone microstructure were measured within six regions of interest (ROIs) spanning from the proximal to the distal aspects of the calcaneal crescent as shown in Figure 3. ROIs were rectangular prisms with $10 \times 10 \times 2$ mm³ dimensions selected in the middle of the specimens' depths. The dimensions of the ROIs were defined to ensure uniform sampling and sufficient coverage of trabecular bone based on the authors' experience. This size was chosen based on pilot tests by the authors to balance resolution and representativeness while avoiding the inclusion of cortical bone and soft tissue regions that may confound microstructural analysis. Additionally, cortical bone thickness (Ct.Th) and bone radiodensity in HU were measured within the proximal and distal sections of the calcaneal crescent (ROI 7 and ROI 8), that are manually traced, as shown in Figure 3b. A three-dimensional (3D) local adaptive grayscale thresholding algorithm was used to segment the bone pixels from the marrow and other soft tissue pixels within each selected ROI. Local thickness was calculated at each voxel using the distance transform performed on the segmented images. Specifically, the local trabecular and corti-

cal thickness in a 3D fashion equals the diameter of the largest sphere covered within the trabeculae and cortical boundaries, respectively. Likewise, the local trabecular space was determined by the diameter of the largest sphere covered within the intertrabecular space. All image processing was performed using MATLAB codes developed in-house.

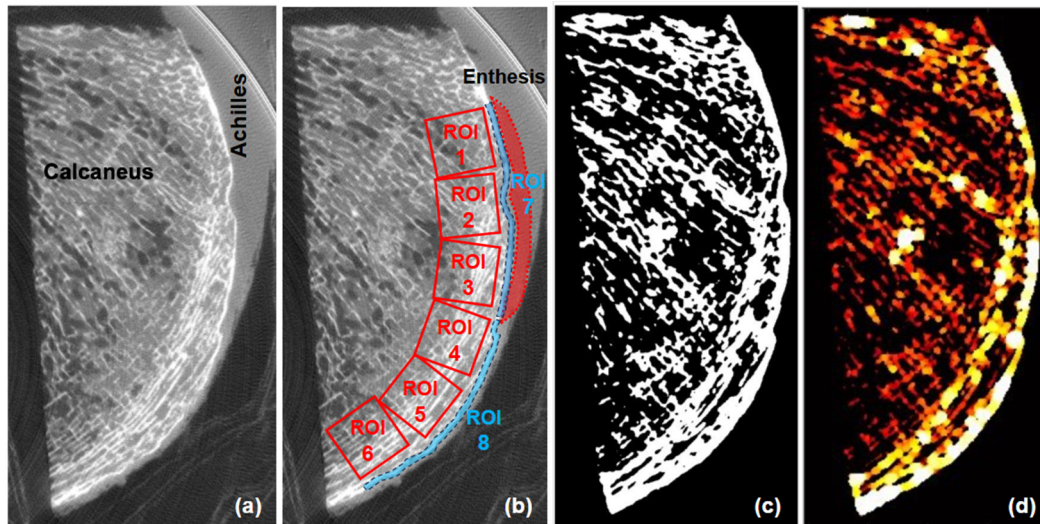


Figure 3. (a) A representative Achilles tendon-calcaneus specimen sagittal image using micro-CT at 50-micron voxel size. (b) The observation areas of the calcaneal bone selected over a cropped image with increased contrasts. ROIs 1, 2, and 3 divided the trabecular bone into three areas beneath the enthesion, and ROIs 4, 5, and 6 divided the trabecular bone into three areas in the plantar region distal to the enthesion. ROIs 7 and 8 divided the cortical bone into two areas: the enthesal and plantar regions. (c) The segmented bone image and (d) the local thickness map was calculated using MATLAB.

2.4. Statistical Correlations

Spearman's correlation coefficients were calculated between the elastic modulus of Achilles tendon enthesion and micro-CT-based measured bone microstructure, including BV/TV, Tb.Th, Tb.Sp, Ct.Th, and bone radiodensity for the different bone ROIs. The differences in these parameters between the ROIs were investigated using ANOVA statistics. Correlations and differences with p -values below 0.05 were considered significant. The statistical analyses were performed using SPSS (version 29, IBM Corp, Armonk, NY, USA).

3. Results

3.1. Bone Microstructure and CT Values

Figure 3a shows a sagittal image of a representative Achilles tendon-calcaneus specimen imaged using micro-CT. The trabecular bone of the calcaneal crescent is arranged in a characteristic direction, with the trabeculae predominantly oriented in a direction almost parallel to the long axis of the Achilles tendon. Figure 3b shows the observation area of the calcaneus, with ROIs 1, 2, and 3 dividing the trabecular bone into three areas in the enthesal region, and ROIs 4, 5, and 6 dividing the trabecular bone into three areas in the plantar region beyond the enthesion. ROIs 7 and 8 divide the cortical bone along the crescent into the enthesal and plantar regions, respectively. Figure 3c,d display the segmented bone and local thickness map calculated using MATLAB, respectively.

Table 1 and Figure 4 present the mean values of BV/TV, Tb.Th, bone radiodensity, and Tb.Sp for six ROIs in the trabecular bone. No significant differences are found between ROIs except for Tb.Sp between ROIs 2 and 6. Bone radiodensity shows an increasing trend toward ROI 3. The Tb.Th and Tb.Sp both demonstrate an increasing trend toward ROI 6.

Table 1. Comparison of Bone Microstructure and CT Values Across Different ROIs.

ROI	BV/TV (%)	Tb.Th (μm)	Bone Radiodensity (HU)	Tb.Sp (μm)
1	46.6 \pm 6.4	601 \pm 198	362 \pm 217	666 \pm 76
2	48.4 \pm 6.1	617 \pm 98	397 \pm 238	646 \pm 76
3	46.2 \pm 3.9	588 \pm 101	415 \pm 247	674 \pm 83
4	47.1 \pm 6.2	574 \pm 90	403 \pm 242	683 \pm 170
5	42.5 \pm 10.4	608 \pm 106	366 \pm 227	788 \pm 281
6	43.1 \pm 13.5	704 \pm 165	360 \pm 227	833 \pm 252

This table presents the mean values and standard deviations (\pm SD) of Bone microstructure and CT values across different ROIs. abbreviations: Bone Volume to Total Volume (BV/TV), Trabecular Thickness (Tb.Th), Bone Radiodensity in Hounsfield Units (HU), Trabecular Separation (Tb.Sp), and Region of Interest (ROI).

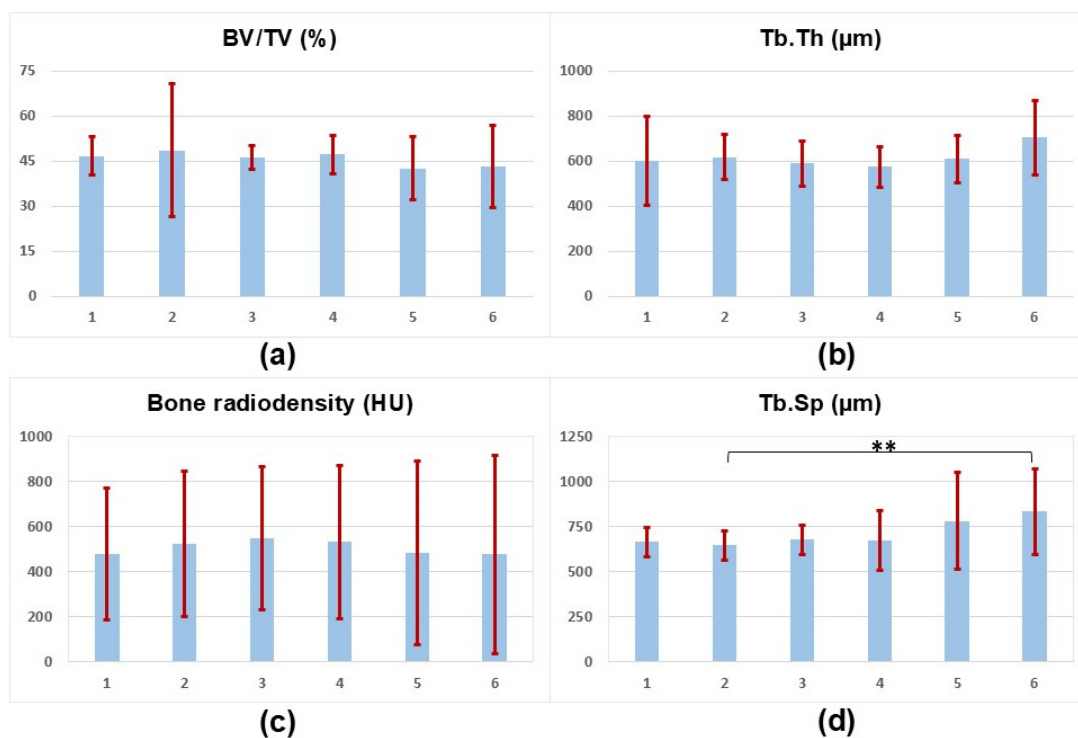


Figure 4. Bar charts illustrating the mean values of (a) Bone Volume to Total Volume (BV/TV), (b) Trabecular Thickness (Tb.Th), (c) Bone radiodensity in Hounsfield Units (HU), and (d) Trabecular Separation (Tb.Sp) for six Regions of Interest (ROIs). Error bars in red represent standard deviations. ** indicated a statistically significant difference.

The Ct.Th in ROIs 7 and 8 are 1006 ± 207 and 1040 ± 190 μm , respectively. The bone radiodensity in ROIs 7 and 8 are 591 ± 346 and 562 ± 334 HU, respectively. No statistically significant differences are observed in Ct.Th and bone radiodensity in HU between those cortical bone regions.

3.2. Correlation between Achilles Elastic Modulus and Bone Microstructure

Figure 5 shows scatter plots and linear trend lines for the average Hayes' modulus within entheses against the average bone microstructure within ROI 1 to ROI 6. Bone microstructure in ROI 1 and ROI 2 (proximal and middle enthesal regions, respectively) shows no significant correlation. In ROI 3, which is in the distal enthesal region, there are significant positive correlations between entheses elastic modulus and trabecular bone thickness ($R = 0.702$, $p < 0.001$). In ROI 4, which is in the proximal plantar region, there is a significant positive correlation between the elastic modulus and bone thickness ($R = 0.507$, $p = 0.027$). In ROI 5 and ROI 6 (middle and distal plantar regions, respectively), there are no significant correlations with entheses elastic modulus. No significant correlations are found between elasticity modulus and cortical bone measures.

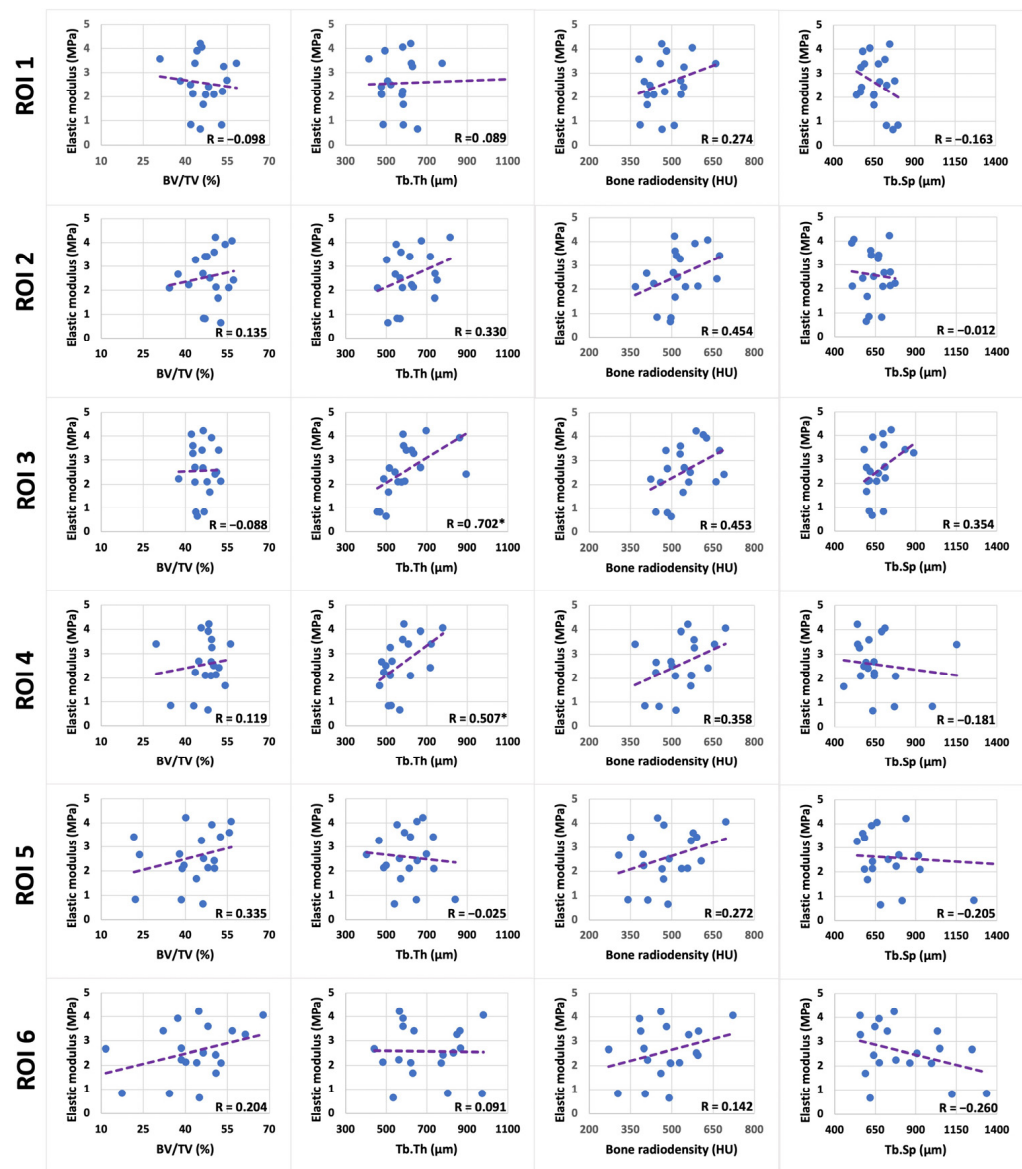


Figure 5. Scatter plots and linear trend lines for the average Hayes' elastic modulus within the enthesis of Achilles tendon against the average trabecular bone microstructural parameters within ROI 1 to ROI 6 in calcaneal crescent. abbreviations: Bone Volume to Total Volume (BV/TV), Trabecular Thickness (Tb.Th), Bone Radiodensity in Hounsfield Units (HU), Trabecular Separation (Tb.Sp), and Region of Interest (ROI).

4. Discussion

This study reveals positive correlations between the mechanical properties of the Achilles tendon enthesis and the bone microstructure in the calcaneal crescent. The enthesis elastic modulus correlated significantly with the trabecular bone thickness in the distal enthesal region and the proximal plantar region but not elsewhere, indicating potential regional differences in load transfer and adaptive bone remodeling.

These findings are consistent with existing literature on the biomechanical aspects of the Achilles tendon and its attachment to the calcaneus. The calcaneal crescent is a region of trabecular bone that is directly influenced by the tensile forces transmitted by the Achilles tendon [9,24]. Previous studies have reported reduced calcaneal bone mineral density due to injury to the Achilles tendon in humans [28]. Several studies have shown that the physical loading environment influences the formation of bone architecture and bone density [9,21,25]. This literature agrees with the principle of Wolff's law that theorizes that

the changes in bone formation and direction follow the force application [10,22]. Visual inspection also shows that the trabeculae of the calcaneal crescent are oriented predominantly in a characteristic direction, aligning nearly parallel to the fibers of the Achilles tendon. Experimental evidence suggests that trabeculae develop along the direction of maximum principal stress [29], indicating that the trabecular pattern observed in the calcaneal crescent is likely influenced by the stress environment.

The observed correlation between the elastic modulus of the enthesis and the trabecular bone thickness beneath the calcaneal enthesis was significant at the distal but not the proximal part. This finding is consistent with previous studies that have reported a higher incidence of bone spurs and enthesal pathology at the distal part of the Achilles tendon insertion [30]. This likely suggests a regional variation in the load transfer and adaptation mechanisms, consistent with the curvature of the calcaneus and the oblique orientation of the tendon fibers [30]. In a histological study, Milz et al. reported that the calcaneal Achilles tendon attachment site showed a trabecular bone structure arranged in a fixed direction [9]. They concluded that this structure was oriented by mechanical stress. Our study also confirmed visually in micro-CT images that the bone microstructure beneath the calcaneal enthesis is roughly aligned along the direction of the Achilles tendon axis. Therefore, assessing the regional variation in the bone microstructure at the Achilles tendon insertion may provide insight into the local stress distribution and metabolic conditions of the tendon-bone complex. While correlations between the enthesis mechanical properties and trabecular bone thickness were observed in specific regions, no significant associations were found for other microstructural parameters such as BV/TV and Tb.Sp. This lack of association may be attributed to the relatively small sample size and potential confounding factors that were not controlled for in this ex vivo study. Moreover, differences in bone adaptation mechanisms across various anatomical regions may contribute to these findings, necessitating further research to elucidate the biomechanical significance of these parameters.

No significant correlation was observed between enthesis mechanics and the cortical bone measures in this study. However, several pieces of evidence suggest that mechanical stress modifies the contour and shape of cortical and subchondral bone beneath the tendon, affecting load transfer [22,31,32]. The limited number of specimens, inadequate image resolution, and our less-than-optimal image segmentation method might be why we could not observe such relationships. Future studies could explore the use of high-field gradient MRI systems, such as 9.4 T MRI, in combination with histological and molecular imaging techniques for the evaluation of tendon and enthesis properties. Such systems may provide higher-resolution images, facilitating the reconstruction and assessment of small-scale anatomical and compositional details [33].

The results of this study may have potential clinical implications for the management of enthesopathies and other tendon-bone interface pathologies. The correlation between enthesis stiffness and trabecular bone microstructure suggests that alterations in tendon mechanical properties, as seen in tendinopathy or aging, may contribute to changes in bone structure, potentially predisposing patients to stress fractures or bone spur formation. Although this should be examined comprehensively in future well-designed studies, assessing both tendon and bone properties could be crucial in early diagnosis and targeted therapeutic interventions.

The current study is limited in several aspects. First, a relatively small number of samples was included (19 sections from 10 donors), which is common in pilot ex vivo studies. Moreover, the visual inspection of the tendon-enthesis specimens indicated that all samples were roughly normal without any obvious degeneration or tearing. Future investigations are suggested to include more specimens with various degrees of degeneration to enhance the generalizability of this study. Second, the elastic modulus measurement on the studied specimens was performed using indentation tests by sagittal compression forces, which do not simulate real-life in vivo forces and physiological conditions. Future investigation should include tensile mechanical tests of the tendon to be compared with bone properties.

However, the enthesis portion often does course around the calcaneus partially during dorsiflexion and plantarflexion of the ankle, resulting in compression forces [1,34]. Third, the study did not measure the biochemical composition of the Achilles tendon, its fiber direction, and density, as well as the trabecular bone orientation and shape, which may provide additional information on the biomechanical and pathophysiological aspects of the tendon-bone complex. Fourth, the study did not account for the potential confounding factors that may affect the Achilles tendon and the trabecular bone structure, such as age, sex, body mass index, physical activity level, medical history, and medication use, which should be investigated in future studies.

5. Conclusions

This study investigates the correlation between the mechanical properties of the Achilles tendon enthesis and bone microstructure in the calcaneal crescent. The results showed that the mechanical properties of Achilles tendon enthesis were positively correlated with the trabecular bone microstructure in the calcaneal crescent. The effect of Achilles tendon enthesis on the calcaneal bone microstructure beneath the enthesis was more pronounced in the distal than the proximal part, suggesting regional differences in the mechanisms of the load transfer and adaptation. Although these findings suggest a relationship between enthesis mechanics and bone microstructure, the limited sample size and moderate correlation coefficients indicate that these results should be interpreted cautiously. Further investigations with larger sample sizes and a more comprehensive analysis of additional microstructural parameters are necessary to confirm these associations and better understand the biomechanical implications of these findings.

Author Contributions: Conceptualization, K.D., D.M. and S.J.; methodology, K.D., C.B.C. and S.J.; software, S.J.; validation, K.D., D.M. and S.J.; formal analysis, K.D. and S.J.; investigation, K.D., D.M., B.N., A.M.A. and S.J.; resources, S.S. and C.B.C.; data curation, K.D., D.M., S.S. and S.J.; writing—original draft preparation, K.D.; writing—review and editing, K.D., T.Y., K.Y.C., C.B.C. and S.J.; visualization, K.D.; supervision, T.Y., C.B.C. and S.J.; project administration, C.B.C. and S.J.; funding acquisition, C.B.C. and S.J. All authors have read and agreed to the published version of the manuscript.

Funding: The authors acknowledge grant support from the National Institutes of Health (K01AR080257 and 5P30AR073761), Veterans Affairs Clinical Science and Rehabilitation R&D (I01BX005952), JSPS Overseas Challenge Program for Young Researchers, and Academic Senate Grant of University of California, San Diego (RG106833).

Institutional Review Board Statement: This study was conducted in accordance with the Declaration of Helsinki, and approved by the Institutional Review Board of the University of California, San Diego (protocol code #804315; approval date: 28 June 2022).

Informed Consent Statement: A requirement for informed consent was waived.

Data Availability Statement: Patient data cannot be shared under the approved study protocol.

Conflicts of Interest: The authors declare no conflicts of interest.

References

1. Benjamin, M.; Ralphs, J.R. Fibrocartilage in tendons and ligaments--an adaptation to compressive load. *J. Anat.* **1998**, *193 Pt 4*, 481–494. [[CrossRef](#)]
2. Benjamin, M.; McGonagle, D. The anatomical basis for disease localisation in seronegative spondyloarthritis at entheses and related sites. *J. Anat.* **2001**, *199 Pt 5*, 503–526. [[CrossRef](#)]
3. Rossetti, L.; Kuntz, L.A.; Kunold, E.; Schock, J.; Müller, K.W.; Grabmayr, H.; Stolberg-Stolberg, J.; Pfeiffer, F.; Sieber, S.A.; Burgkart, R.; et al. The microstructure and micromechanics of the tendon-bone insertion. *Nat. Mater.* **2017**, *16*, 664–670. [[CrossRef](#)]
4. Hu, Y.; Birman, V.; Deymier-Black, A.; Schwartz, A.G.; Thomopoulos, S.; Genin, G.M. Stochastic interdigitation as a toughening mechanism at the interface between tendon and bone. *Biophys. J.* **2015**, *108*, 431–437. [[CrossRef](#)]
5. Deymier, A.C.; An, Y.; Boyle, J.J.; Schwartz, A.G.; Birman, V.; Genin, G.M.; Thomopoulos, S.; Barber, A.H. Micro-mechanical properties of the tendon-to-bone attachment. *Acta Biomater.* **2017**, *56*, 25–35. [[CrossRef](#)]

6. Moffat, K.L.; Sun, W.H.; Pena, P.E.; Chahine, N.O.; Doty, S.B.; Ateshian, G.A.; Hung, C.T.; Lu, H.H. Characterization of the structure-function relationship at the ligament-to-bone interface. *Proc. Natl. Acad. Sci. USA* **2008**, *105*, 7947–7952. [[CrossRef](#)]
7. Genin, G.M.; Kent, A.; Birman, V.; Wopenka, B.; Pasteris, J.D.; Marquez, P.J.; Thomopoulos, S. Functional grading of mineral and collagen in the attachment of tendon to bone. *Biophys. J.* **2009**, *97*, 976–985. [[CrossRef](#)]
8. Sevvick, J.L.; Abusara, Z.; Andrews, S.H.; Xu, M.; Khurshid, S.; Chatha, J.; Hart, D.A.; Shrive, N.G. Fibril deformation under load of the rabbit Achilles tendon and medial collateral ligament femoral entheses. *J. Orthop. Res.* **2018**, *36*, 2506–2515. [[CrossRef](#)]
9. Milz, S.; Rufai, A.; Buettner, A.; Putz, R.; Ralphs, J.R.; Benjamin, M. Three-dimensional reconstructions of the Achilles tendon insertion in man. *J. Anat.* **2002**, *200 Pt 2*, 145–152. [[CrossRef](#)]
10. Benjamin, M.; Toumi, H.; Ralphs, J.R.; Bydder, G.; Best, T.M.; Milz, S. Where tendons and ligaments meet bone: Attachment sites ('entheses') in relation to exercise and/or mechanical load. *J. Anat.* **2006**, *208*, 471–490. [[CrossRef](#)]
11. Freedman, B.R.; Gordon, J.A.; Soslow, L.J. The Achilles tendon: Fundamental properties and mechanisms governing healing. *Muscles Ligaments Tendons J.* **2014**, *4*, 245–255. [[CrossRef](#)]
12. Cook, J.L.; Purdam, C.R. Is tendon pathology a continuum? A pathology model to explain the clinical presentation of load-induced tendinopathy. *Br. J. Sports Med.* **2009**, *43*, 409–416. [[CrossRef](#)]
13. Sundararajan, P.P.; Wilde, T.S. Radiographic, clinical, and magnetic resonance imaging analysis of insertional Achilles tendinopathy. *J. Foot Ankle Surg.* **2014**, *53*, 147–151. [[CrossRef](#)]
14. Lukas, C.; Ruffoni, D.; Lambers, F.M.; Schulte, F.A.; Kuhn, G.; Kollmannsberger, P.; Weinkamer, R.; Müller, R. Mineralization kinetics in murine trabecular bone quantified by time-lapsed in vivo micro-computed tomography. *Bone* **2013**, *56*, 55–60. [[CrossRef](#)]
15. Galatz, L.M.; Ball, C.M.; Teefey, S.A.; Middleton, W.D.; Yamaguchi, K. The outcome and repair integrity of completely arthroscopically repaired large and massive rotator cuff tears. *J. Bone Jt. Surg. Am.* **2004**, *86*, 219–224. [[CrossRef](#)]
16. Schulte, F.A.; Ruffoni, D.; Lambers, F.M.; Christen, D.; Webster, D.J.; Kuhn, G.; Müller, R. Local mechanical stimuli regulate bone formation and resorption in mice at the tissue level. *PLoS ONE* **2013**, *8*, e62172. [[CrossRef](#)]
17. Christen, P.; Ito, K.; Ellouz, R.; Boutroy, S.; Sornay-Rendu, E.; Chapurlat, R.D.; van Rietbergen, B. Bone remodelling in humans is load-driven but not lazy. *Nat. Commun.* **2014**, *5*, 4855. [[CrossRef](#)]
18. Cheong, V.S.; Roberts, B.C.; Kadirkamanathan, V.; Dall'Ara, E. Bone remodelling in the mouse tibia is spatio-temporally modulated by oestrogen deficiency and external mechanical loading: A combined in vivo/in silico study. *Acta Biomater.* **2020**, *116*, 302–317. [[CrossRef](#)]
19. Tits, A.; Ruffoni, D. Joining soft tissues to bone: Insights from modeling and simulations. *Bone Rep.* **2020**, *14*, 100742. [[CrossRef](#)]
20. Mullender, M.G.; Huiskes, R. Proposal for the regulatory mechanism of Wolff's law. *J. Orthop. Res.* **1995**, *13*, 503–512. [[CrossRef](#)]
21. Ruff, C.; Holt, B.; Trinkaus, E. Who's afraid of the big bad Wolff?: "Wolff's law" and bone functional adaptation. *Am. J. Phys. Anthropol.* **2006**, *129*, 484–498. [[CrossRef](#)]
22. Tits, A.; Plougonven, E.; Blouin, S.; Hartmann, M.A.; Kaux, J.F.; Drion, P.; Fernandez, J.; van Lenthe, G.H.; Ruffoni, D. Local anisotropy in mineralized fibrocartilage and subchondral bone beneath the tendon-bone interface. *Sci. Rep.* **2021**, *11*, 16534. [[CrossRef](#)]
23. Ficek, K.; Filipek, J.; Ficek, J.; Muzalewska, M.; Humpa, F. Calcaneal CT is a useful tool for identifying Achilles tendon disorders: A pilot study. *J. Orthop. Surg. Res.* **2017**, *12*, 139. [[CrossRef](#)]
24. Finkenstaedt, T.; Siritwanarangsun, P.; Statum, S.; Biswas, R.; Anderson, K.E.; Bae, W.C.; Chung, C.B. The Calcaneal Crescent in Patients With and Without Plantar Fasciitis: An Ankle MRI Study. *AJR Am. J. Roentgenol.* **2018**, *211*, 1075–1082. [[CrossRef](#)]
25. Frost, H.M. Wolff's Law and bone's structural adaptations to mechanical usage: An overview for clinicians. *Angle Orthod.* **1994**, *64*, 175–188.
26. Jerban, S.; Afsahi, A.M.; Ma, Y.; Moazamian, D.; Statum, S.; Lombardi, A.F.; Kakos, L.; Dorthe, E.; Dlima, D.; Du, J.; et al. Correlations between elastic modulus and ultrashort echo time (UTE) adiabatic T1ρ relaxation time (UTE-Adiab-T1ρ) in Achilles tendons and entheses. *J. Biomech.* **2023**, *160*, 111825. [[CrossRef](#)]
27. Hayes, W.C.; Keer, L.M.; Herrmann, G.; Mockros, L.F. A mathematical analysis for indentation tests of articular cartilage. *J. Biomech.* **1972**, *5*, 541–551. [[CrossRef](#)]
28. Wren, T.A.; Yerby, S.A.; Beaupré, G.S.; Carter, D.R. Influence of bone mineral density, age, and strain rate on the failure mode of human Achilles tendons. *Clin. Biomech.* **2001**, *16*, 529–534. [[CrossRef](#)]
29. Hart, N.H.; Nimphius, S.; Rantalainen, T.; Ireland, A.; Siafarikas, A.; Newton, R.U. Mechanical basis of bone strength: Influence of bone material, bone structure and muscle action. *J. Musculoskelet. Neuronal Interact.* **2017**, *17*, 114–139.
30. McGonagle, D.; Wakefield, R.J.; Tan, A.L.; D'Agostino, M.A.; Toumi, H.; Hayashi, K.; Emery, P.; Benjamin, M. Distinct topography of erosion and new bone formation in achilles tendon enthesitis: Implications for understanding the link between inflammation and bone formation in spondylarthritis. *Arthritis Rheum.* **2008**, *58*, 2694–2699. [[CrossRef](#)]
31. Li, G.; Yin, J.; Gao, J.; Cheng, T.S.; Pavlos, N.J.; Zhang, C.; Zheng, M.H. Subchondral bone in osteoarthritis: Insight into risk factors and microstructural changes. *Arthritis Res. Ther.* **2013**, *15*, 1–12. [[CrossRef](#)] [[PubMed](#)]
32. Goldring, S.R. Alterations in periarticular bone and cross talk between subchondral bone and articular cartilage in osteoarthritis. *Ther. Adv. Musculoskelet. Dis.* **2012**, *4*, 249–258. [[CrossRef](#)] [[PubMed](#)]

33. Pušnik, L.; Lechner, L.; Serša, I.; Cvetko, E.; Haas, P.; Jengojan, S.A.; Snoj, Ž. 3D fascicular reconstruction of median and ulnar nerve: Initial experience and comparison between high-resolution ultrasound and MR microscopy. *Eur. Radiol. Exp.* **2024**, *8*, 100. [[CrossRef](#)] [[PubMed](#)]
34. Luyckx, T.; Verstraete, M.; De Roo, K.; De Waele, W.; Bellemans, J.; Victor, J. Digital image correlation as a tool for three-dimensional strain analysis in human tendon tissue. *J. Exp. Orthop.* **2014**, *1*, 7. [[CrossRef](#)]

Disclaimer/Publisher's Note: The statements, opinions and data contained in all publications are solely those of the individual author(s) and contributor(s) and not of MDPI and/or the editor(s). MDPI and/or the editor(s) disclaim responsibility for any injury to people or property resulting from any ideas, methods, instructions or products referred to in the content.